Environmental Science & Technology

pubs.acs.org/est

Article

Gas-Phase Oxidation Rates and Products of 1,2-Dihydroxy Isoprene

Kelvin H. Bates, James D. Cope, and Tran B. Nguyen*

Cite This: *Environ. Sci. Technol.* 2021, 55, 14294−14304

Read Online

ACCESS | Metrics & More | Article Recommendations | Supporting Information

ABSTRACT: 1,2-Dihydroxy isoprene (1,2-DHI), a product of isoprene oxidation from multiple chemical pathways, is produced in the atmosphere in large quantities; however, its chemical fate has not been comprehensively studied. Here, we perform chamber experiments to investigate its gas-phase reactions. We find that the reactions of 1,2-DHI with OH radicals and ozone are rapid (k_{OH} = 8.0 (±1.3) × 10^{-11} cm^3 $molecule^{-1}$ s^{-1}; k_{O3} = 7.2 (±1.1) × 10^{-18} cm^3 $molecule^{-1}$ s^{-1}). Reaction with OH, which dominates 1,2-DHI loss, leads primarily to fragmentation and radical recycling; major products under both high- and low-NO conditions include hydroxyacetone, glycolaldehyde, and 2,3-dihydroxy-2-methyl-propanal (DHMP). Radical-terminating hydroperoxide formation from the peroxy radical (RO_2) reaction with HO_2 and organonitrate formation from RO_2 + NO are not observed in the gas phase, possibly due to low volatility; constraints for their branching ratios are instead derived by mass balance. We also measure secondary organic aerosol mass yields from 1,2-DHI (0−23%) and show that oxidation in the presence of aqueous particles leads to formic and acetic acid production. Finally, we incorporate results into GEOS-Chem, a global chemical transport model, to compute the global production (25.3 Tg a^{-1}) and gas-phase loss (20.2 Tg a^{-1}) of 1,2-DHI and show that its oxidation provides non-negligible contributions to the atmospheric budgets of hydroxyacetone, glycolaldehyde, hydroxymethyl hydroperoxide, formic acid, and DHMP.

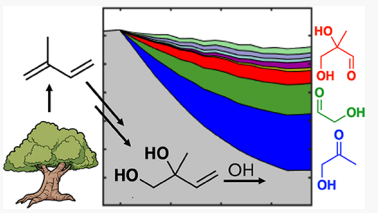

KEYWORDS: *isoprene, VOC, oxidation, photochemistry, SOA, biogenic*

INTRODUCTION

Isoprene (2-methyl-1,3-butadiene), a hydrocarbon emitted to the atmosphere predominantly by broad-leaved plants, reacts rapidly in the gas phase with the hydroxyl radical (OH). Its complex subsequent chemistry, recently reviewed by Wennberg et al.,[1] has important local and global repercussions on ozone pollution[2,3] and secondary organic aerosol (SOA) formation,[4,5] as well as the tropospheric HO_x (OH + HO_2) and NO_x (NO + NO_2) budgets.[6,7] The immense magnitude of global isoprene emissions—at ∼500 Tg a^{-1}, it is comparable to emissions of methane[8]—underscores the importance of understanding even minor channels and intermediates in its oxidation mechanism.

One such compound is 1,2-dihydroxyisoprene (1,2-DHI; 2-methyl-3-butene-1,2-diol). The widespread observation of isoprene-derived 2-methyltetrols (2-MT) in ambient organic aerosol led to early interest in 1,2-DHI as a potential SOA precursor since it was assumed to be a necessary intermediate in the oxidative mechanism from isoprene to 2-MT.[9−21] However, chamber experiments found low yields both of 1,2-DHI from isoprene and of 2-MT from 1,2-DHI.[21−24] The discovery of isoprene epoxydiols (IEPOX) as a product of gas-phase isoprene oxidation,[25] and subsequent observation of efficient SOA formation from IEPOX uptake to aqueous aerosol,[26,27] provided evidence of an alternative pathway to 2-MT formation. More recently, there is renewed interest in DHI based on its production from other channels within the isoprene photochemical cascade.

Figure 1 summarizes the atmospheric pathways of 1,2-DHI production from isoprene. In the gas phase, its dominant source is the reaction of the isoprene 1-hydroxy-2-peroxy radical (1,2-ISOPOO·, the most abundant peroxy radical isomer from isoprene's oxidation by OH[1]) with other organic peroxy radicals (RO_2). The branching ratio to alcohol formation in this reaction is uncertain but likely low[28] and is only available in the reaction of 1,2-ISOPOO· with radicals that have the peroxy group attached to a primary or secondary carbon. Overall, this makes 1,2-DHI formation in the gas phase a minor but non-negligible fate of isoprene photooxidation (1.2% yield globally,[7] assuming a 50% branching ratio from 1,2-ISOPOO· + CH_3O_2[29] and a 12.5% branching ratio from 1,2-ISOPOO· + other primary and secondary RO_2[30]).

Two new pathways to 1,2-DHI formation, both mediated by aqueous particles, have recently been documented. First, 1-hydroxy-2-hydroperoxy isoprene (1,2-ISOPOOH), an abundant first-generation product of isoprene oxidation in low-NO_x conditions, can partition into cloud or aerosol droplets and react with HSO_3^-, forming SO_4^{2-} and 1,2-DHI.[31,32] Second, 1-hydroxy-2-nitrooxy isoprene (1,2-IHN), a minor product of the 1,2-ISOPOO· + NO reaction, rapidly hydrolyzes in cloud

Received: June 23, 2021
Revised: September 8, 2021
Accepted: September 9, 2021
Published: October 7, 2021

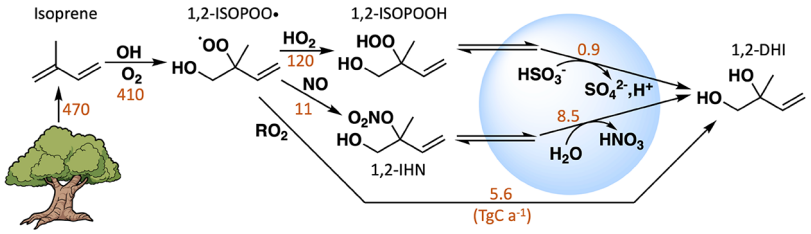

Figure 1. Mechanism for the formation of 2-methylbut-3-ene-1,2-diol (1,2-DHI) in the atmosphere. Annual global carbon fluxes through each pathway (TgC a^{-1}), shown in brown, are calculated from a GEOS-Chem simulation (see text).

Table 1. Initial Conditions for Experiments Performed in This Work[a]

expt.	type	1,2-DHI (ppb)	H_2O_2 (ppm)	O_3 (ppb)	NO (ppb)	CH_3ONO (ppb)	propene (ppb)	cyclohexane (ppm)	RH (%)	T (°C)	seed area ($\mu m^2/cm^3$)	seed mass ($\mu g/m^3$)
1	OH rate	58	2.5				360		<5	22		
2	OH rate	23				66	360		<5	22		
3	OH rate	61				2020	5100		<5	22		
4	Ox. (OH, NO)	48	2.5		194				<5	22		
5	Ox. (OH, HO_2)	54	2.5						<5	22		
6	Ox. (OH, H-shift)	102				40			<5	35		
7	Ox. (OH, RO_2)	403	2.5						<5	22		
8	Ox. (O_3, dry)	144		720				50	<5	22		
9	Ox. (O_3, wet)	166		980				50	48	22		
10	SOA (OH, NO)	123	2.5		561				50	22	9700	370
11	SOA (OH, HHO_2)	116	3.5						51	22	5280	250
12	SOA (OH, H-shift)	100				40			48	35	5940	260
13	Ox. (O_3, dry)	143		775					<5	22	7330	340
14	Ox. (O_3, wet)	104		650					56	22	7220	320

[a]See Table S1 for additional details and modeled reactant concentrations.

and aerosol particles to produce 1,2-DHI and inorganic nitrate.[33] In both cases, the diol is sufficiently volatile to partition back to the gas phase, where it can undergo further oxidative chemistry. Both the ISOPOOH + HSO_3^- and 1,2-IHN hydrolysis pathways are much more efficient for the 1,2 isomers of each precursor than the corresponding 3,4 isomers. Furthermore, the 1,2 isomers are more abundantly produced than the 3,4 in the gas phase; as a result, atmospheric formation of 3,4-DHI is estimated to be an order of magnitude smaller than 1,2-DHI. Together with the gas-phase formation, these new pathways lead to a global 1,2-DHI yield of 3.2% from isoprene[31−33] or a total annual production (25.3 Tg a^{-1}) similar to the combined global emissions of C_6−C_9 aromatic hydrocarbons (22.4 Tg a^{-1}).[34]

These newly identified 1,2-DHI sources, the magnitude of its global production, and the detail with which the isoprene oxidation mechanism can now be represented in models,[7,35] all indicate a need to determine the atmospheric fate of 1,2-DHI. Previous chamber experiments targeting 1,2-DHI did not investigate its gas-phase oxidation products or rates.[21−24] Here, we perform environmental chamber experiments on synthetic 1,2-DHI to investigate its gas-phase chemistry and SOA production under a range of atmospheric conditions, including OH- and ozone-initiated oxidation and the isolation of various peroxy radical fates. Using data from these experiments to constrain a kinetic model, we estimate reaction rates and product yields. Finally, we implement these parameters in a global chemical transport model to investigate the influence of these new reaction pathways on tropospheric chemical outcomes.

MATERIALS AND METHODS

Materials. Hydrogen peroxide (H_2O_2, 50 wt % in H_2O), ammonium sulfate ($(NH_4)_2SO_4$, ≥99%), propene gas (≥99%), and cyclohexane (≥99%) were procured from Sigma Aldrich, and a nitric oxide (NO, 200 ppm ±1% in N_2) primary standard was from Praxair. Methyl nitrite (CH_3ONO) was synthesized following the procedures of Taylor et al.[36] from the reaction of methanol (≥99.8%, Sigma Aldrich) and $NaNO_2$ (≥99%, Sigma Aldrich) in the presence of sulfuric acid (40%, Sigma Aldrich). 1,2-DHI was prepared from hydrolysis of 2-methyl-2-vinyloxirane (95%, Sigma Aldrich) as described by Wang et al.[24] and Ruppert and Becker.[22] Its identity and purity were confirmed by ^1H NMR (Figure S1).

Chamber Experiments. Experiments were performed in a 10 m^3 environmental chamber made of fluorinated ethylene propylene (Teflon-FEP, DuPont) housed in a climate-controlled enclosure with UV-reflective interior siding and 72 individual 40 W broadband blacklights centered at 350 nm (Sylvania). The chamber was operated in batch mode and flushed with purified dried air (100 L min^{-1}) for at least 12 h between experiments. Experiments were performed at ambient pressure (~755 Torr), with the chamber temperature held at 22 ± 1 °C unless otherwise noted.

Initial conditions for chamber experiments are listed in Table 1. For each experiment, humidity and temperature were first adjusted to the desired values; experiments 6 and 12 were performed with the chamber heated to 35 °C. Reactants were then introduced to the chamber as described below followed by pulses of purified dried air and 1 h of static equilibration to ensure that the chamber was well-mixed. For ozonolysis experiments (8, 9, 13, and 14), this mixing period preceded the injection of ozone, which marked the start of the experiment;

https://doi.org/10.1021/acs.est.1c04177
Environ. Sci. Technol. 2021, 55, 14294−14304

for all other experiments, the UV lights were turned on after equilibration to initialize photochemistry.

1,2-DHI and H_2O_2 were separately introduced to the chamber by placing the desired volume into a small glass bulb and gently heating the bulb to 40 °C with a water bath while flowing ultra zero air (Airgas) at 4 L min^{-1} through the bulb into the chamber. Methyl nitrite and propene were added to the chamber by filling an evacuated, shrouded 500 mL glass bulb to the required pressure, backfilling the balance with UHP N_2 (Airgas), and similarly flowing the bulb's contents into the chamber with ultra zero air. For experiments 10−14, seed particles were introduced to the chamber by atomizing a solution of 0.06 M $(NH_4)_2SO_4$ with UHP N_2 (Airgas) at 35 psi through a ^{210}Po neutralizer and a heated wet-walled denuder to ensure an even charge distribution and particle deliquescence in humid experiments. Ozone was injected into the chamber by flowing O_2 (Matheson Gas) through an ozone generator (A2Ozone, Inc.) directly into the chamber.

Control experiments identical to experiments 8−14 but without 1,2-DHI were also performed. Diameter-dependent rates of particle wall loss from seeded controls were used to correct particle observations in the experiments with 1,2-DHI as described by Schwantes et al.[37] Small increases in the concentrations of formic and acetic acids, presumably from reactions of organics deposited on walls, were observed in some controls. The background organic acid formation in controls was subtracted from the observed rates in the corresponding experiments with 1,2-DHI on a per-experiment basis. Background rates of formic acid production from the controls for experiments 11 and 12 were used to correct the observed yields in experiments 7 and 6, respectively. Additional control experiments quantifying any vapor wall loss or photolysis of 1,2-DHI, i.e., identical to experiment 5 but without lights or without H_2O_2, showed no measurable loss of 1,2-DHI within uncertainty under both dry (<5% RH) and humid (50% RH) conditions.

Instrumentation. Temperature and humidity in the environmental chamber were continuously monitored with a Vaisala membrane probe. Gases and particles were measured throughout experiments with a suite of instruments connected to the chamber with short (4′−10′) lengths of 1/4″-diameter Teflon (for gases) or stainless steel and conductive (for particles) tubing. Ozone concentrations were monitored with a photometric Thermo Scientific Model 49i O_3 analyzer and nitrogen oxide concentrations with a chemiluminescence Thermo Scientific Model 42i NO-NO_2-NO_x analyzer. A gas chromatograph (Agilent 6890N with a CP 7354 PoraBOND Q column) with a flame ionization detector was used to quantify propene and any potential methyl vinyl ketone (MVK) from 1,2-DHI oxidation, although none was detected above the detection limit of 5 ppb. Particle size and number concentrations between 15 and 670 nm were measured with a scanning mobility particle sizer, consisting of an electrostatic classifier (TSI model 3080) coupled to a condensation particle counter (TSI model 3772), operating at an aerosol flow rate of 0.3 L min^{-1}. Particle volume growth during experiments was converted to mass assuming an SOA density of 1.2 g cm^{-3}.[38]

Mixing ratios of 1,2-DHI and its gas-phase oxidation products were quantified with a custom-built chemical ionization mass spectrometer (CIMS) with a triple-quadrupole mass analyzer (Varian 1200), using CF_3O^- as the reagent ion. Similar instruments have been described in detail previously,[39,40] including humidity-dependent sensitivity calibrations.[27] Here, we measured humidity-dependent sensitivities for hydroxyacetone, glycolaldehyde, formic acid, and acetic acid and used previously published ratios to these sensitivities for other analytes.[41−44] For all such analytes, measured sensitivities matched those estimated from the target compound's dipole moment and polarizability as described previously.[44−46] CF_3O^- interacts with polar analytes (A, with molar mass M) either through clustering (resulting in $[A\cdot CF_3O]^-$, detected at m/z M+85) or through fluoride transfer (resulting in $[A\cdot F]^-$, detected at m/z M+19), the latter of which is more common for acids. The CIMS alternated between a scanning MS mode (m/z 50−250) and a tandem MS mode (MS/MS), in which collision-induced dissociation with argon gas can cause fragmentation of ions to distinguish isobars (e.g., acetic acid and glycolaldehyde) and potentially indicate functional groups. The flow from the chamber to the CIMS inlet was 2 L min^{-1}, and the CIMS inlet flow tube was coated with a hydrophobic Fluoropel coating (Cytonix) to minimize vapor losses prior to detection.

Kinetic Modeling and Product Yield Estimations. We used a simple kinetic model (Mech. S1) to simulate the gas-phase chemistry of 1,2-DHI and its products in each experiment. The mechanism was run on Matlab (MathWorks, Inc.) and used reaction parameters for inorganic and C_1 species from the 2019 JPL Chemical Kinetics and Photochemical Data Evaluation.[47] For larger organic products of 1,2-DHI oxidation, we used rates and branching ratios from the Caltech Isoprene Mechanism.[1] For the reactions of 1,2-DHI and its first-generation peroxy radical intermediates, we adjusted rates and branching ratios to fit the experimental data as described below. Simulations were initialized with the species and environmental conditions listed in Table 1. The model did not include gas−particle interactions and was used only in comparisons with unseeded experiments to confirm that rates and product yields matched gas-phase experimental data.

To quantify the formation yields of observed products, we have to account for their own losses to reactions with OH. Since their OH reaction rates are known,[43,48,49] this can be accomplished by estimating the OH in the chamber from the rate of diol loss and using that to correct the observed product mixing ratios. We then performed an error-weighted regression between the diol loss and corrected product formation to estimate the product yield and its uncertainty.[50] Alternatively, corrections for the loss of products to reactions with OH can be minimized and even ignored when examining only the early stages of diol oxidation, when the diol concentration is much higher than the product concentrations; therefore, the production rate of products is much greater (we used a cutoff of 2× greater) than their loss rates. The error-weighted regression analysis provided similar results to the initial yield analysis, within uncertainty, for all the products investigated here except (in some experiments) hydroxymethyl hydroperoxide (HMHP) and 2,3-dihydroxy-2-methyl-propanal (DHMP), which were lost faster than can be explained by their OH oxidation rates. This implies that other sinks, presumably including photolysis (for HMHP) and wall losses, are significant for these compounds. In these cases, we used only the initial yields.

Global Modeling. Atmospheric simulations of 1,2-DHI chemistry were performed with GEOS-Chem (http://geos-chem.org), a global chemical transport model driven by the Modern-Era Retrospective analysis for Research and Applica-

https://doi.org/10.1021/acs.est.1c04177
Environ. Sci. Technol. 2021, 55, 14294−14304

tions (MERRA-2) assimilated meteorological observations from the NASA Global Modeling and Assimilation Office (GMAO). We used model version 12.8 (DOI: 10.5281/zenodo.3860693), which incorporates a detailed isoprene oxidation mechanism.[7] We further updated the mechanism with the 1,2-IHN hydrolysis and ISOPOOH + HSO_3^- sources of 1,2-DHI as described by Vasquez et al.[33] and Dovrou et al.[31] Isoprene emissions were calculated from the MEGAN v2.1 inventory[8] and scaled uniformly to 535 Tg a^{-1}; all other emissions used the standard HEMCO configuration.[51] Simulations were run at a 2° × 2.5° horizontal resolution with 47 vertical layers for the year 2016, following a year of model spin-up, and all results reported below are annual totals.

RESULTS AND DISCUSSION

Reaction Kinetics. Results from experiments 1−3 were used to quantify the rate of reaction between 1,2-DHI and OH ($k_{OH+1,2\text{-DHI}}$). Because OH was not directly measured, propene was used as a reference compound for kinetic determinations. The second-order rate coefficient of 1,2-DHI photooxidation ($k_{OH+1,2\text{-DHI}}$) was inferred from the observed relative decay rates of propene compared to 1,2-DHI, as shown in Figure 2.

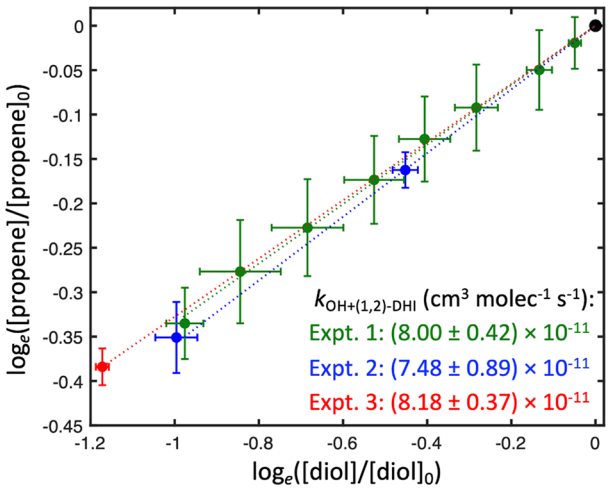

Figure 2. Fractional losses of propene and 2-methylbut-3-ene-1,2-diol (1,2-DHI) in experiments 1−3. Slopes are calculated by error-weighted regression,[50] and $k_{OH+(1,2)\text{-DHI}}$ (bottom right) assume a $k_{OH+propene}$ of 2.68 × 10^{-11} cm^3 $molecule^{-1}$ s^{-1}.[52] Calculated standard deviations incorporate measurement and regression uncertainties but do not include uncertainty in $k_{OH+propene}$.

For each experiment, we calculate a linear regression between the natural log of the fraction of propene remaining and the natural log of the fraction of 1,2-DHI remaining in the chamber, incorporating error in both dimensions.[50] The resulting slope gives the ratio of the two reaction rates with OH. Using a rate constant $k_{OH+propene}$ of 2.68 × 10^{-11} cm^3 $molecule^{-1}$ s^{-1} at 295 K for propene,[52] we calculate $k_{OH+1,2\text{-DHI}}$ to be 8.0 (±1.3) × 10^{-11} cm^3 $molecule^{-1}$ s^{-1} as the error-weighted mean across the three experiments. The standard deviation incorporates measurement and regression uncertainties as well as uncertainty in $k_{OH+propene}$, estimated to be 15%.[52] This fast rate implies a short gas-phase lifetime against OH oxidation of 3.5 h at [OH] = 1 × 10^6 molecules cm^{-3} and 295 K. Our measured rate is identical, within uncertainty, to that of 1,2-ISOPOOH, for which $k_{OH+1,2\text{-ISOPOOH}}$ is 7.5 (±1.2) × 10^{-11} cm^3 $molecule^{-1}$ s^{-1},[53] as expected from the two compounds' close structural similarity.

Because ozone mixing ratios could be directly measured in the chamber, the ozonolysis rate constant ($k_{O3+1,2\text{-DHI}}$) was determined without propene in experiments 8 and 9. Cyclohexane was used as an OH scavenger to ensure that ozonolysis was the only appreciable 1,2-DHI loss pathway. The ozonolysis rate constant ($k_{O3+1,2\text{-DHI}}$) was then determined by adjusting its value in the kinetic model to provide the best possible model-measurement fit. Our measured ozonolysis rate constant of 7.2 (±1.1) × 10^{-18} cm^3 $molecule^{-1}$ s^{-1} at 295 K is in the range of other terminal gas-phase alkenes, as expected (e.g., 9.9 × 10^{-18} cm^3 $molecule^{-1}$ s^{-1} for propene and 4.9 × 10^{-18} cm^3 $molecule^{-1}$ s^{-1} for MVK at 295 K).[48]

Gas-Phase Products. Calculated product molar yields from gas-phase product formation experiments are shown in Table 2. Under all conditions, DHMP production (21−49%) is a major reactive channel. DHMP was first observed as a gas-phase oxidation product from IEPOX,[41] and its own reaction with OH was described by Bates et al.[43] While the DHMP + OH reaction can form a low-yielding product isobaric with 1,2-DHI that could interfere with measurements, our own kinetic modeling and MS/MS fragmentation patterns (Figure S2) indicate that this does not cause appreciable bias during the experiments performed here. As a C_4 compound, DHMP is coproduced with a C_1 compound presumed to be formaldehyde (not observable by our instruments). The other dominant products in OH-initiated experiments were the C_2 compound glycolaldehyde and the C_3 compound hydroxyacetone, which were always produced in roughly identical yields (19−69%); their structures and yields imply that they are from the same product channel in the OH-oxidation of 1,2-DHI. In ozonolysis experiments, major products include DHMP, hydroxyacetone, HMHP, formic acid, and an unknown compound observed at m/z 169 in the CF_3O^- CIMS (presumed to be $C_4H_6O_6$; see below). Small yields of formic acid were also observed in OH-initiated experiments targeting H-shift and RO_2 + RO_2 chemistry (experiments 6 and 7).

Table 2. Measured Product Yields from Experiments 4−9[a]

experiment		product yields (%, molar)					
no.	oxidation pathway	$C_4H_8O_3$ (DHMP)	hydroxyacetone	glycolaldehyde	HMHP	formic Acid	m/z 169
4	OH, NO	32 ± 2	69 ± 5	66 ± 4			
5	OH, HO_2	21 ± 2	38 ± 9	40 ± 7			
6	OH, H-shift	48 ± 5	20 ± 3	19 ± 2		14 ± 11	
7	OH, RO_2	28 ± 5	42 ± 8	44 ± 9		11 ± 4	
8	O_3 (dry)	49 ± 3	15 ± 3		29 ± 2	13 ± 1	8.8 ± 0.3
9	O_3 (wet)	46 ± 3	14 ± 3		34 ± 2	46 ± 11	8.9 ± 0.3

[a]Reported standard deviations include only uncertainties in regression analysis, not in CIMS calibrations.

https://doi.org/10.1021/acs.est.1c04177
Environ. Sci. Technol. 2021, 55, 14294−14304

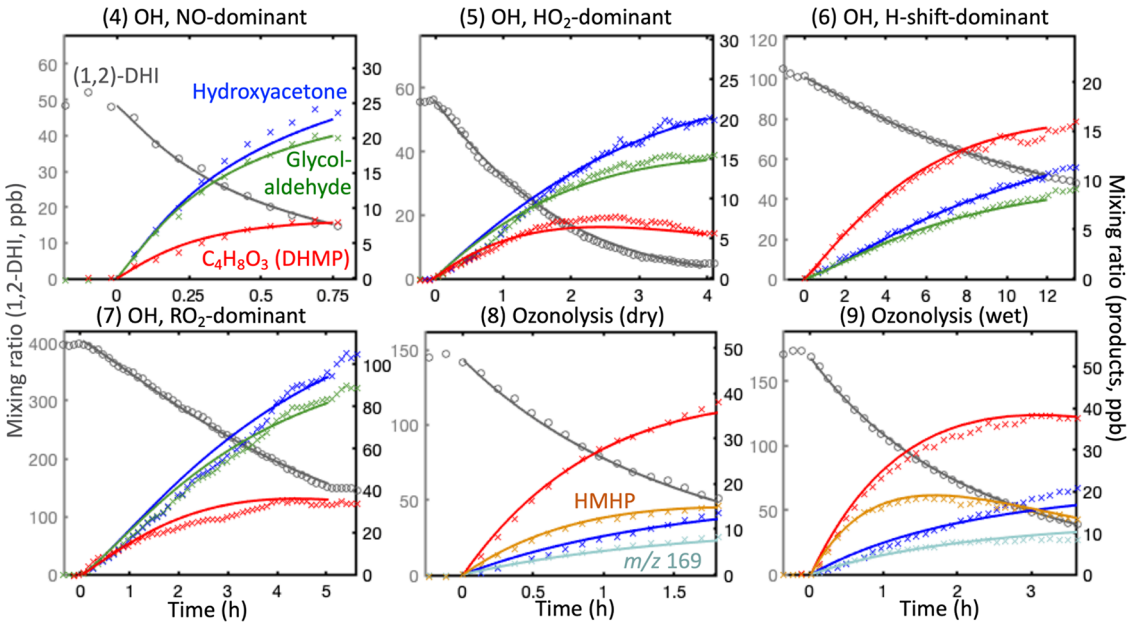

Figure 3. Measured (points) and modeled (lines) mixing ratios of the precursor and reaction products in the OH- and ozone-initiated oxidation of 2-methylbut-3-ene-1,2-diol (1,2-DHI) in experiments 4−9, under various oxidation conditions described above each panel. 1,2-DHI mixing ratios are shown on the left axes, while those of products are shown on the right; scales differ between panels.

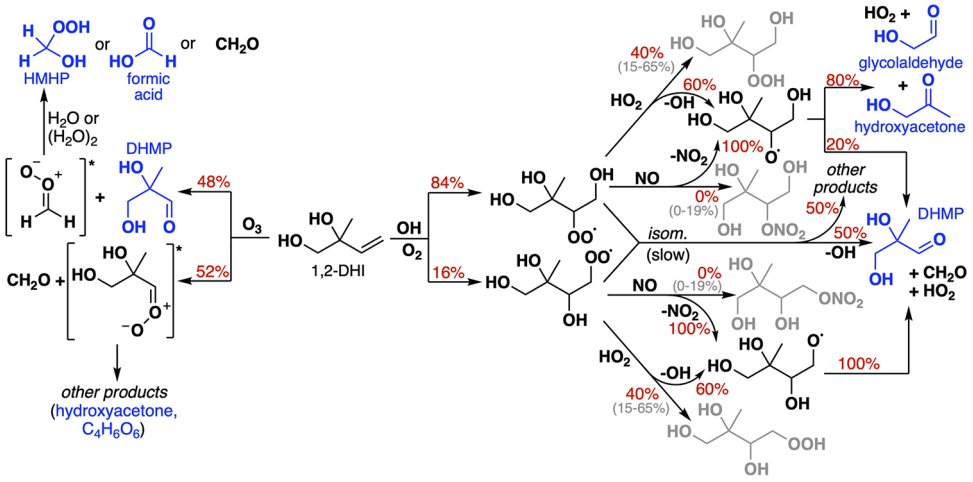

Figure 4. Proposed mechanism for the OH- and O_3-initiated oxidation of 2-methylbut-3-ene-1,2-diol (1,2-DHI) in the gas phase. Branching ratios from the best-fit kinetic model are shown in red. Species in blue are measured by CIMS in this work. Species in gray are not observed, though the CIMS is sensitive to them, and are assumed to partition to the chamber walls or particles; uncertainty bounds for their branching ratios are shown in parentheses.

Figure 3 shows the loss of 1,2-DHI and formation of key products in experiments 4−9, the results from which were used to estimate product yields from each oxidative pathway of 1,2-DHI and to constrain the branching ratios in the kinetic model accordingly. To convert from observed product to branching ratios for each chemical pathway, we use the kinetic model described above. We initialize the model with estimated branching ratios from structure−activity relationships (SAR) developed by Wennberg et al.[1] for organonitrate formation from RO_2 + NO, hydroperoxide formation from RO_2 + HO_2, and fragmentation pathways of alkoxy radicals. We use estimated intramolecular isomerization rates based on the H-shift type (hydroxy or α-hydroxy) and distance as described by Möller et al.[54] This initial model, the mechanism for which is shown in Figure S3, includes formation routes for all the observed products from OH-initiated experiments but does not adequately reproduce the yields of those products; as described below, it tends to overestimate radical-terminating hydroperoxide and organonitrate formation from the reactions of RO_2 with HO_2 and NO, respectively, and to underestimate fragmentation product channels, especially the formation of hydroxyacetone and glycolaldehyde. Thus, we adjust branching ratios and H-shift rates using observed yields in Table 2 until all the data can be satisfactorily fit by the kinetic model, as shown in Figure 3 and described in greater detail below.

Figure 4 shows the resulting branching ratios in the final mechanism from the kinetic model, which is reproduced fully in the Supporting Information. For the OH-initiated oxidation of 1,2-DHI, we observe no production of 2-hydroxy-2-methylbut-3-en-1-al, predicted to account for 3% of the OH reactivity via abstraction of an α-hydroxy hydrogen, nor do we observe any MVK from hydroxyl abstraction.[53] High observed

https://doi.org/10.1021/acs.est.1c04177
Environ. Sci. Technol. 2021, 55, 14294−14304

yields of hydroxyacetone and glycolaldehyde from experiment 4 necessitate either an increase in the isomer branching ratio for the major (secondary) RO_2 radical formation from 75 to 84% or an increase in the fraction of secondary alkoxy radicals fragmenting to C_2/C_3 products (vs C_4/C_1) from 80 to 90%. We opt for the former because an analogous reaction of 1,2-ISOPOOH with OH also produces secondary peroxy radicals at a much higher fraction (95%) than predicted by SAR,[1] such that an 84% branching ratio of the 1,2-DHI + OH reaction to the secondary RO_2 will be in good agreement, but note that our results do not rule out the latter possibility.

The most notable deviation from SAR predictions in the final mechanism is the decreased branching ratios for radical-terminating pathways from RO_2 + NO and RO_2 + HO_2. Despite predicted yields of 17−19%, we observe no organonitrate formation in experiment 4 and instead observe enough DHMP, hydroxyacetone, and glycolaldehyde to account for 100% of the reacted 1,2-DHI. Wennberg et al.[1] noted, in developing the SAR used here for organonitrate branching ratios, that nearby oxygen-containing functional groups tend to diminish organonitrate yields and that the combined effects of these substituents remained highly uncertain for polyfunctionalized compounds. A recent SAR developed by Jenkin et al.[55] proposed even stronger suppression of organonitrate formation from oxygen-containing functional groups, based on substantial experimental evidence,[56−68] which would revise our initial estimate down from 17−19% to 9−10%. We hypothesize, consistent with Wennberg et al.[1] and Jenkin et al.,[55] that the cumulative effect of the three hydroxyl groups on the peroxy radical from 1,2-DHI is to substantially suppress organonitrate formation, and we use the best fit organonitrate branching ratio of 0% in our kinetic model, although the true range of yields may be between 0 and 19%.

Similarly, we observe no C_5 trihydroxy-hydroperoxide, which is presumed to be the dominant product from RO_2 + HO_2, in experiment 5. As with RO_2 + NO, it has previously been shown that the presence of additional functional groups tends to increase the branching ratio of the radical-propagating channel in RO_2 + HO_2 reactions, particularly for carbonyl-containing compounds.[44,69−71] It is possible that the abundant functionalization of the peroxy radical from 1,2-DHI similarly suppresses hydroperoxide formation. Because the observed DHMP, hydroxyacetone, and glycolaldehyde are able to account for 60% of reacted 1,2-DHI in experiment 5, we revise the RO_2 + HO_2 hydroperoxide yield down to 40% from the SAR-predicted 75−85% to match our observed yields. We apply this reduction uniformly to both RO_2 isomers; the two may differ slightly, but the uniform branching ratios are best able to fit our observed ratio of DHMP to the C_2/C_3 compounds.

Both the C_5 trihydroxy-nitrate and C_5 trihydroxy-hydroperoxide may be formed during NO-dominated and HO_2-dominated experiments, respectively, but be unobserved due to losses to walls, aerosol, and the CIMS inlet. Indeed, previous studies have observed similar C_5 tetrafunctionalized compounds from the oxidation of isoprene derivatives using instruments designed to measure lower-volatility compounds than the CF_3O^- CIMS used here.[72,73] Both the C_5 trihydroxy-nitrate and C_5 trihydroxy-hydroperoxide have sufficiently low volatility to undergo substantial surface losses, with saturation vapor pressures of 18.24 and 1.44 $\mu g\ m^{-3}$, respectively, as estimated by the EVAPORATION model.[74] Furthermore, St. Clair et al.[53] used a similar CF_3O^- CIMS to the instrument used here and did not observe the C_5 dihydroxy-dihydroperoxide that Krechmer et al.[72] and Liu et al.[73] measured, though all three investigated the ISOPOOH + OH reaction under low-NO conditions. For this reason, we cannot rule out the C_5 products' formation. We estimate their branching ratios from the carbon balance of the unseeded experiments, from which 0% may be assignable to the trihydroxy-nitrate and 40% to the trihydroxy-hydroperoxide. Based on the uncertainties in the CIMS calibrations of 1,2-DHI and its other products, the C_5 trihydroxy-nitrate branching ratio from the NO pathway could still be as high as the 17−19% predicted by SAR, and the C_5 trihydroxy-hydroperoxide branching ratio could be as low as 15% or as high as 65%. Thus, we can assign the following range of yields within experimental uncertainty: 0−19% for the trihydroxy-nitrate and 15−65% for the trihydroxy-hydroperoxide.

Experiment 6 was designed to emphasize the importance of H-shift reactions.[75,76] CH_3ONO was used as an OH precursor with only 15% of the environmental chamber lights to minimize reactive radical concentrations, while the temperature was increased to 35 °C, which should increase H-shift rates by factors of 2−5.[54,75] Low levels of both HO_2 (<65 ppt) and NO (<300 ppt) in these experiments provide longer RO_2 lifetimes, during which H-shifts may occur. Peroxy radicals from 1,2-DHI have a number of possible H-shift routes, shown in full detail in Figures S4 and S5. The route expected to dominate for both isomers involves the shift of the α-hydroxy hydrogen, which would produce either a C_5 dihydroxy-hydroperoxy-aldehyde ($C_5H_{10}O_5$) or a C_4 hydroxy-hydroperoxy-aldehyde ($C_4H_8O_4$) upon reaction with O_2. However, neither of these products are observed. It is possible, similarly to the hydroperoxide from RO_2 + HO_2, that these compounds indeed form but are rapidly lost to surfaces; the small observed formic acid yield may derive from reactions on these surfaces. However, the observed DHMP and C_2/C_3 products are inconsistent with the presence of a dominant H-shift pathway to unique products, even at elevated temperatures. Instead, an elevated DHMP to hydroxyacetone ratio (and, equivalently, DHMP to glycolaldehyde) relative to the ratio observed in other OH-initiated experiments suggests an H-shift channel to form DHMP, which could arise from a (1,5)-H-shift of a hydroxyl hydrogen or a (1,4)-H-shift of an α-hydroxy hydrogen. We find that the observations are best explained with an isomerization rate of 0.1 s^{-1} at T = 308 K (assumed to have a temperature dependence of $e^{(-5000/T)}$ for the kinetic model) and a DHMP yield of 50%, with the remainder assumed to make an unobserved product that partitions to walls or particles.

While the reactions of RO_2 with other peroxy radicals are not shown in Figure 4, we include this pathway in the kinetic model, and experiment 7 was designed to maximize its contribution. However, the rates and branching ratios of these reactions are not well-constrained (and can differ between isomers), and the modeled fraction of RO_2 reacting via RO_2 + RO_2 in experiment 7 is highly sensitive to the chosen rate.[28] Observed yields are consistent with a bulk rate of $k_{RO2+RO2} = 5 \times 10^{-13}$ cm^3 $molecule^{-1}$ s^{-1} and a branching ratio to 2RO + O_2 of 100%. We do not observe any evidence of an appreciable pathway to produce ROH + $R_{(-H)}$=O, which should be detectable by the CF_3O^- CIMS, nor do we observe any dimers, though these would presumably be lost rapidly to surfaces. Observed product yields from the alkoxy radical fragmentation relative to those in experiment 5 are not consistent with a

https://doi.org/10.1021/acs.est.1c04177
Environ. Sci. Technol. 2021, 55, 14294−14304

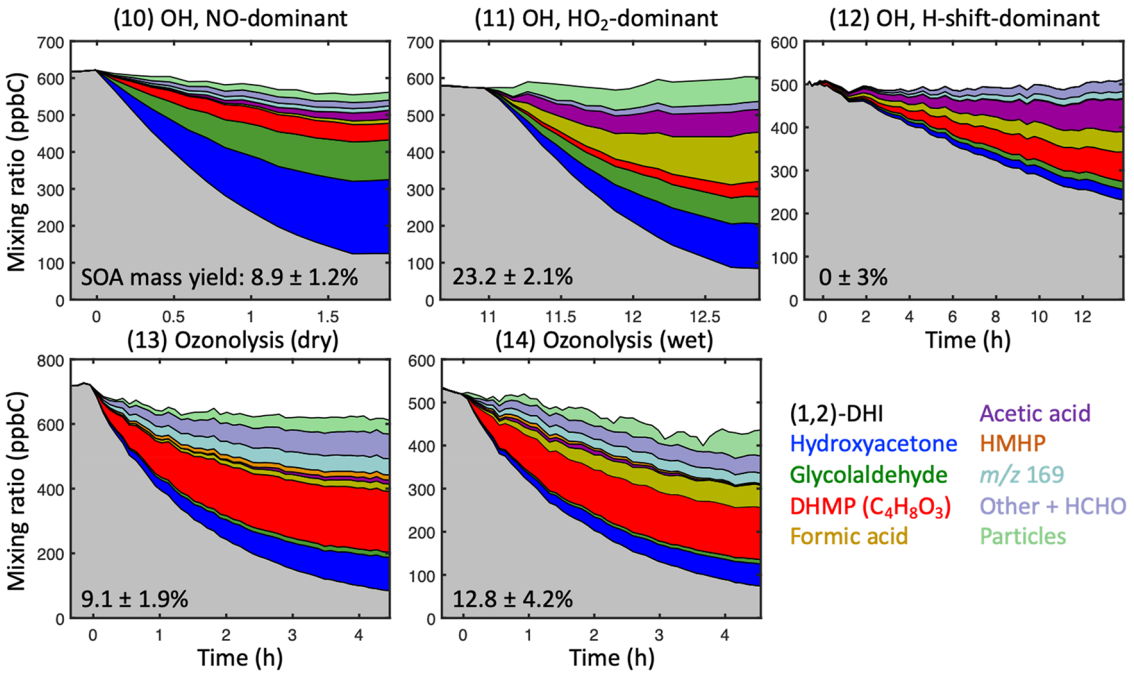

Figure 5. Stacked measured mixing ratios of all observed species in seeded experiments (nos. 10−14). Mixing ratios are expressed in ppbC such that the total would theoretically remain constant across the experiment (assuming that all products are measured). To convert from particle mass to ppbC, SOA is assumed to have the formula $C_5H_{11}NO_6$ in experiment 10 and $C_5H_{12}O_5$ in all other experiments. "Others" include small (<2%) yields of some C_5 compounds measured by CIMS, along with the presumed (unmeasured) CH_2O coproduct of DHMP ($C_4H_8O_3$). Stack order is consistent between panels.

faster $RO_2 + RO_2$ rate, unless the increased rate is balanced by a decreased $2RO + O_2$ branching ratio, presumably balanced by unobserved production of $ROH + R_{(-H)}{=}O$ or dimers.

Finally, experiments 8 and 9 investigated 1,2-DHI ozonolysis. HMHP yields in both wet and dry conditions are consistent with a 55% branching ratio to form the C_1 stabilized Criegee intermediate (sCI), based on the balance of subsequent reactions between the C_1 CI and both H_2O and $(H_2O)_2$,[42] which is similar to comparable terminal alkenes (e.g., 58% for isoprene[1]). The expected coproduct of DHMP is observed to form with a 48% yield. The other reaction route, to form the C_4 CI, has a number of available pathways, including unimolecular isomerizations and decompositions. We measure a 14−15% yield of HAC, presumably from this decomposition, as well as an unknown compound observed at m/z 169. Assuming a sensitivity equivalent to that of 1,2-DHI, the yield of this compound is 9% under either wet or dry conditions. MS/MS fragmentation (Figure S6) indicates that the observed mass is from a fluoride transfer in the CF_3O^- CIMS, suggesting that the compound has a molar mass of 150 (the most likely formula corresponds to $C_4H_6O_6$) and may be an acid.

Aerosol Formation. While no particle formation was observed in experiments 4−9, the lack of carbon closure from gaseous compounds in most of the experiments suggested that some products were lost to surfaces, which might instead be taken up by particles in the ambient atmosphere. Experiments 10−14 were therefore performed with added deliquesced ammonium sulfate seed aerosol, such that the particle growth could be measured to quantify the contributions of these additional pathways and the SOA yields under various reactive conditions. High seed surface areas (>5000 μm^2 cm^{-3}) and moderate relative humidity (~50%) were used to ensure that semivolatile and water-soluble compounds would partition to particles. High seed surface areas are necessary to ensure that partitioning of semivolatile gas-phase compounds to particles dominates over partitioning to chamber walls, as it has been shown that an insufficient seed surface area in chamber experiments will underestimate SOA yields.[37,77,78] Although the particle-phase compounds were not chemically speciated as part of this work, reasonable assumptions can be made about their chemical composition. Assuming $C_5H_{11}NO_6$ as an average molecular formula for SOA from high-NO chemistry, and $C_5H_{12}O_5$ otherwise, enables an estimate of the particle carbon content, from which we can determine whether these experiments achieve carbon closure.

Figure 5 shows the carbon balance in seeded experiments 10−14. In all cases, the observed gas-phase species and particle mass come within 16% of achieving the carbon balance (9% for OH experiments). The missing carbon mass could be due to uncertainties in CIMS sensitivity, compounds that were not detected (such as HCHO), or higher-than-expected product sinks. We see accelerated loss of HMHP and DHMP in the humid seeded experiments, suggesting that they react on or partition into aqueous particles, possibly contributing to particle mass or yields of volatile products that may not be accounted for in the carbon balance closures. HMHP is known to hydrolyze quickly on surfaces,[79] and DHMP may behave similarly to other aldehydes such as glyoxal that reactively uptakes onto wet ammonium sulfate particles.[80,81] SOA mass yields, also shown in Figure 5, range between 0 and 23.2% under various experimental conditions. The mass yields presented here likely differ from what may form in the atmosphere since the ambient seed area and composition (water, organics, inorganics, and metals) will differ from those used in the seeded experiments herein, and semivolatile products may deposit or be oxidized before partitioning to the aerosol phase. Further study is necessary to determine the

https://doi.org/10.1021/acs.est.1c04177
Environ. Sci. Technol. 2021, 55, 14294−14304

chemistry of these SOA formation pathways and whether they are kinetically limited or based on equilibrium partitioning.

Although the seeded experiments achieve mass balance within measurement uncertainties, the observed particle mass is too small to fully account for the compounds such as the C_5 trihydroxy-hydroperoxide from RO_2 + HO_2 chemistry that we expect to contribute to secondary aerosol formation. Instead, as Figure 5 shows, we also observe enhanced yields of gas-phase formic and acetic acids in the presence of particles, which make up much of the previously unaccounted-for mass. We hypothesize that this is due to particle-phase or heterogeneous oxidation of some 1,2-DHI products, including the C_5 trihydroxy-hydroperoxide, in seeded experiments due to partitioning of H_2O_2. Another isoprene derivative, 2-methyltetrol, has recently been shown to react rapidly with OH in the aqueous phase to produce large yields of formic and acetic acids, which can subsequently revolatilize and be observed in the gas phase.[82] The more rapid loss of DHMP observed in seeded experiments suggests that it may also take part in this particle-mediated reactive pathway. Future work isolating the aqueous reactivity of 1,2-DHI products will be needed to quantify these reaction rates and products.

Atmospheric Implications. To investigate the effects of 1,2-DHI chemistry on the global atmosphere, we implement the reaction rates and product yields measured here into a modified version of GEOS-Chem. As described above, we augment the GEOS-Chem isoprene mechanism with the additional 1,2-IHN hydrolysis and 1,2-ISOPOOH + HSO_3^- sources of 1,2-DHI from Vasquez et al.[33] and Dovrou et al.[31] We then add the gas-phase reactions of 1,2-DHI and its peroxy radicals as constrained by our chamber experiments. A list of the added reactions is provided in the Supporting Information. Deposition parameters for 1,2-DHI in GEOS-Chem are set equal to those of ISOPOOH, but the reactivity factor for dry deposition is reduced by a factor of three, based on lower observed deposition velocities for alcohols and hydroxycarbonyls relative to hydroperoxides.[83]

As shown in Figure 1, we find that 25.3 Tg a^{-1} of 1,2-DHI is produced from the atmospheric oxidation of isoprene: 37% from the gas-phase reactions of isoprene-derived peroxy radicals with other organic peroxy radicals, 6% from 1,2-ISOPOOH + HSO_3^-, and 57% from 1,2-IHN hydrolysis. The overall production is geographically diverse because the dominant sources—RO_2 + RO_2 and 1,2-IHN hydrolysis—occur under low-NO and high-NO conditions, respectively. However, these production numbers remain somewhat uncertain, especially from the RO_2 + RO_2 pathway, as the rates and branching ratios are poorly constrained.[1] Within plausible uncertainty ranges, the RO_2 + RO_2 pathway could produce between 2 and 18 Tg a^{-1} of 1,2-DHI globally. While 1,2-IHN yields and hydrolysis rates are better constrained, their implementation in GEOS-Chem is imperfect. In particular, we ignore particle-phase chemistry of 1,2-DHI, which may provide an additional loss process prior to revolatilization and reaction in the gas phase, and instead assume that equilibrium partitioning between the gas phase and the unreactive particle phase is achieved instantaneously. As a result, GEOS-Chem may overestimate the flux of carbon through the gas-phase reactive pathways of 1,2-DHI. Further experimental constraints on RO_2 + RO_2 chemistry and on aqueous reaction pathways would help alleviate these uncertainties.

Globally, we find that 90% of 1,2-DHI reacts in the gas phase, with the remainder undergoing depositional losses. Of this fraction, 90% reacts with OH and 10% with ozone. These reactions, and the subsequent oxidation of DHMP formed from 1,2-DHI, produce 12.7 Tg a^{-1} of hydroxyacetone (13% of the global total from all pathways), 11.4 Tg a^{-1} of DHMP (44%), 5.9 Tg a^{-1} of glycolaldehyde (10%), 1.6 Tg a^{-1} of formic acid (3.1%), 0.4 Tg a^{-1} of HMHP (2%), 4.0 Tg a^{-1} of formaldehyde (0.3%), and 11.8 Tg a^{-1} of the C_5 trihydroxy-hydroperoxide. Because we do not account for the particle-mediated production of formic and acetic acids observed in experiments 10−14, we likely underestimate the source of these compounds, which are chronically underestimated in GEOS-Chem and other models,[84−86] from 1,2-DHI. We also do not account for SOA formation from 1,2-DHI or its products in GEOS-Chem, but based on the experimental yields from each RO_2 pathway and the fraction of 1,2-DHI-derived RO_2 reacting by each pathway in GEOS-Chem, we calculate a global SOA source of 1.5 TgC a^{-1} from 1,2-DHI based on the results of this chamber study, which would increase the isoprene-derived SOA source in the model by 2.5%;[7] however, condensation and deposition sinks of semivolatile gases in the atmosphere will differ from our laboratory conditions, and further study is necessary to constrain this pathway under ambient conditions.

■ ASSOCIATED CONTENT

Supporting Information

The Supporting Information is available free of charge at https://pubs.acs.org/doi/10.1021/acs.est.1c04177.

^{1}H NMR of 1,2-dihydroxy isoprene (1,2-DHI); CIMS MS/MS analysis; additional mechanistic figures; table of further details and model output for each experiment performed in this work; list of species and reactions included in the kinetic model (PDF)

■ AUTHOR INFORMATION

Corresponding Author

Tran B. Nguyen − *Department of Environmental Toxicology, University of California Davis, Davis, California 95616, United States;* orcid.org/0000-0001-9206-4359; Email: tbn@ucdavis.edu

Authors

Kelvin H. Bates − *Department of Environmental Toxicology, University of California Davis, Davis, California 95616, United States; Center for the Environment, Harvard University, Cambridge, Massachusetts 02138, United States;* orcid.org/0000-0001-7544-9580

James D. Cope − *Department of Environmental Toxicology, University of California Davis, Davis, California 95616, United States*

Complete contact information is available at: https://pubs.acs.org/10.1021/acs.est.1c04177

Notes

The authors declare no competing financial interest.

Chamber data used in this study are publicly available on the Index for Chamber Atmospheric Research in the United States (ICARUS) at https://icarus.ucdavis.edu/ (experiment DOIs 10.5065/9rb1-pn14, 10.5065/ysde-gf76, 10.5065/n05n-7591, 10.5065/hw9w-1v28, 10.5065/vhd5-6b13, 10.5065/9evw-

https://doi.org/10.1021/acs.est.1c04177
Environ. Sci. Technol. 2021, 55, 14294−14304

sx58, 10.5065/yz1w-m302, 10.5065/6pqc-xn69, 10.5065/jd0m-tf11, 10.5065/f8se-yx39, 10.5065/fma6-bb53, 10.5065/8v2d-y796, 10.5065/dw1r-kz32, 10.5065/4w8d-8a56, 10.5065/0vaw-2k23, and 10.5065/g7hr-fg72).

■ ACKNOWLEDGMENTS

We gratefully acknowledge funding from the National Science Foundation under grant AGS-1656889 through the Atmospheric Chemistry Program and the California Agricultural Experiment Station grant CAD-ETX-2345-H through the USDA National Institute of Food and Agriculture. We thank Dr. Xuan Fu for help with the 1,2-DHI synthesis.

■ REFERENCES

(1) Wennberg, P. O.; Bates, K. H.; Crounse, J. D.; Dodson, L. G.; McVay, R. C.; Mertens, L. A.; Nguyen, T. B.; Praske, E.; Schwantes, R. H.; Smarte, M. D.; St Clair, J. M.; Teng, A. P.; Zhang, X.; Seinfeld, J. H. Gas-Phase Reactions of Isoprene and Its Major Oxidation Products. *Chem. Rev.* **2018**, *118*, 3337−3390.

(2) Paulot, F.; Henze, D. K.; Wennberg, P. O. Impact of the isoprene photochemical cascade on tropical ozone. *Atmos. Chem. Phys.* **2012**, *12*, 1307−1325.

(3) Squire, O. J.; Archibald, A. T.; Griffiths, P. T.; Jenkin, M. E.; Smith, D.; Pyle, J. A. Influence of isoprene chemical mechanism on modelled changes in tropospheric ozone due to climate and land use over the 21st century. *Atmos. Chem. Phys.* **2015**, *15*, 5123−5143.

(4) Carlton, A. G.; Wiedinmyer, C.; Kroll, J. H. A review of secondary organic aerosol (SOA) formation from isoprene. *Atmos. Chem. Phys.* **2009**, *9*, 4987−5005.

(5) Stadtler, S.; Kühn, T.; Schröder, S.; Taraborrelli, D.; Schultz, M. G.; Kokkola, H. Isoprene-derived secondary organic aerosol in the global aerosol-chemistry-climate model ECHAM6.3.0-HAM2.3-MOZ1.0. *Geosci. Model Dev.* **2018**, *11*, 3235−3260.

(6) Romer, P. S.; Duffey, K. C.; Wooldridge, P. J.; Allen, H. M.; Ayres, B. R.; Brown, S. S.; Brune, W. H.; Crounse, J. D.; de Gouw, J.; Draper, D. C.; Feiner, P. A.; Fry, J. L.; Goldstein, A. H.; Koss, A.; Misztal, P. K.; Nguyen, T. B.; Olson, K.; Teng, A. P.; Wennberg, P. O.; Wild, R. J.; Zhang, L.; Cohen, R. C. The lifetime of nitrogen oxides in an isoprene-dominated forest. *Atmos. Chem. Phys.* **2016**, *16*, 7623−7637.

(7) Bates, K. H.; Jacob, D. J. A new model mechanism for atmospheric oxidation of isoprene: Global effects on oxidants, nitrogen oxides, organic products, and secondary organic aerosol. *Atmos. Chem. Phys.* **2019**, *19*, 9613−9640.

(8) Guenther, A. B.; Jiang, X.; Heald, C. L.; Sakulyanontvittaya, T.; Duhl, T.; Emmons, L. K.; Wang, X. The Model of Emissions of Gases and Aerosols from Nature version 2.1 (MEGAN 2.1): an extended and updated framework for modeling biogenic emissions. *Geosci. Model Dev.* **2012**, *5*, 1471−1492.

(9) Claeys, M.; Graham, B.; Vas, G.; Wang, W.; Vermeylen, R.; Pashynska, V.; Cafmeyer, J.; Guyon, P.; Andreae, M. O.; Artaxo, P.; Maenhunt, W. Formation of secondary organic aerosols through photooxidation of isoprene. *Science* **2004**, *303*, 1173−1176.

(10) Claeys, M.; Wang, W.; Ion, A. C.; Kourtchev, I.; Gelencsér, A.; Maenhaut, W. Formation of secondary organic aerosols from isoprene and its gas-phase oxidation products through reaction with hydrogen peroxide. *Atmos. Environ.* **2004**, *38*, 4093−4098.

(11) Ion, A. C.; Vermeylen, R.; Kourtchev, I.; Cafmeyer, J.; Chi, X.; Gelencsér, A.; Maenhaut, W.; Claeys, M. Polar organic compounds in rural $PM_{2.5}$ aerosols from K-puszta, Hungary, during a 2003 summer field campaign: Sources and diel variations. *Atmos. Chem. Phys.* **2005**, *5*, 1805−1814.

(12) Edney, E. O.; Kleindienst, T. E.; Jaoui, M.; Lewandowski, M.; Offenberg, J. H.; Wang, W.; Claeys, M. Formation of 2-methyltetrols and 2-methylglyceric acid in secondary organic aerosol from laboratory irradiated isoprene/NO_x/SO_2/air mixtures and their detection in ambient $PM_{2.5}$ samples collected in the eastern US. *Atmos. Environ.* **2005**, *39*, 5281−5289.

(13) Schkolnik, G.; Falkovich, A. H.; Rudich, Y.; Maenhaut, W.; Artaxo, P. New analytical method for the determination of levoglucosan, polyhydroxy compounds, and 2-methylerythritol and its application to smoke and rainwater samples. *Environ. Sci. Technol.* **2005**, *39*, 2744−2752.

(14) Kourtchev, I.; Ruuskanen, T.; Maenhaut, W.; Kulmala, M.; Claeys, M. Observation of 2-methyltetrols and related photo-oxidation products of isoprene in boreal forest aerosols from Hyytiälä, Finland. *Atmos. Chem. Phys.* **2005**, *5*, 2761−2770.

(15) Plewka, A.; Gnauk, T.; Brüggemann, E.; Herrmann, H. Biogenic contributions to the chemical composition of airborne particles in a coniferous forest in Germany. *Atmos. Environ.* **2006**, *40*, 103−115.

(16) Clements, A. L.; Seinfeld, J. H. Detection and quantification of 2-methyltetrols in ambient aerosol in the southeastern United States. *Atmos. Environ.* **2007**, *41*, 1825−1830.

(17) Kourtchev, I.; Warnke, J.; Maenhaut, W.; Hoffmann, T.; Claeys, M. Polar organic marker compounds in $PM_{2.5}$ aerosol from a mixed forest site in western Germany. *Chemosphere* **2008**, *73*, 1308−1314.

(18) Chan, M. N.; Surratt, J. D.; Claeys, M.; Edgerton, E. S.; Tanner, R. L.; Shaw, S. L.; Zheng, M.; Knipping, E. M.; Eddingsaas, N. C.; Wennberg, P. O.; Seinfeld, J. H. Characterization and Quantification of Isoprene-Derived Epoxydiols in Ambient Aerosol in the Southeastern United States. *Environ. Sci. Technol.* **2010**, *44*, 4590−4596.

(19) Liang, L.; Engling, G.; Duan, F.; Cheng, Y.; He, K. Characteristics of 2-methyltetrols in ambient aerosol in Beijing, China. *Atmos. Environ.* **2012**, *59*, 376−381.

(20) Karambelas, A.; Pye, H. O. T.; Budisulistiorini, S. H.; Surratt, J. D.; Pinder, R. W. Contribution of Isoprene Epoxydiol to Urban Organic Aerosol: Evidence from Modeling and Measurements. *Environ. Sci. Technol. Lett.* **2014**, *1*, 278−283.

(21) Böge, O.; Miao, Y.; Plewka, A.; Herrmann, H. Formation of secondary organic particle phase compounds from isoprene gas-phase oxidation products: An aerosol chamber and field study. *Atmos. Environ.* **2006**, *40*, 2501−2509.

(22) Ruppert, L.; Becker, K. H. A product study of the OH radical-initiated oxidation of isoprene: formation of C_5-unsaturated diols. *Atmos. Environ.* **2000**, *34*, 1529−1542.

(23) Kleindienst, T. E.; Lewandowski, M.; Offenberg, J. H.; Jaoui, M.; Edney, E. O. The formation of secondary organic aerosol from the isoprene + OH reaction in the absence of NO_x. *Atmos. Chem. Phys.* **2009**, *9*, 6541−6558.

(24) Wang, W.; Iinuma, Y.; Kahnt, A.; Ryabtsova, O.; Mutzel, A.; Vermeylen, R.; Van der Veken, P.; Maenhaut, W.; Herrmann, H.; Claeys, M. Formation of secondary organic aerosol marker compounds from the photooxidation of isoprene and isoprene-derived alkene diols under low-NO_x conditions. *Faraday Discuss.* **2013**, *165*, 261−272.

(25) Paulot, F.; Wunch, D.; Crounse, J. D.; Toon, G. C.; Millet, D. B.; DeCarlo, P. F.; Vigouroux, C.; Deutscher, N. M.; González Abad, G.; Notholt, J.; Warneke, T.; Hannigan, J. W.; Warneke, C.; de Gouw, J. A.; Dunlea, E. J.; De Mazière, M.; Griffith, D. W. T.; Bernath, P.; Jimenez, J. L.; Wennberg, P. O. Importance of Secondary Sources in the Atmospheric Budgets of Formic and Acetic Acids. *Atmos. Chem. Phys.* **2011**, *11*, 1989−2013.

(26) Surratt, J. D.; Chan, A. W. H.; Eddingsaas, N. C.; Chan, M.; Loza, C. L.; Kwan, A. J.; Hersey, S. P.; Flagan, R. C.; Wennberg, P. O.; Seinfeld, J. H. Reactive intermediates revealed in secondary organic aerosol formation from isoprene. *Proc. Natl. Acad. Sci.* **2010**, *107*, 6640−6645.

(27) Nguyen, T. B.; Coggon, M. M.; Bates, K. H.; Zhang, X.; Schwantes, R. H.; Schilling, K. A.; Loza, C. L.; Flagan, R. C.; Wennberg, P. O.; Seinfeld, J. H. Organic aerosol formation from the reactive uptake of isoprene epoxydiols (IEPOX) onto non-acidified inorganic seeds. *Atmos. Chem. Phys.* **2014**, *14*, 3497−3510.

(28) Orlando, J. J.; Tyndall, G. S. Laboratory studies of organic peroxy radical chemistry: an overview with emphasis on recent issues of atmospheric significance. *Chem. Soc. Rev.* **2012**, *41*, 6294−6317.

https://doi.org/10.1021/acs.est.1c04177
Environ. Sci. Technol. 2021, 55, 14294−14304

(29) Jenkin, M. E.; Boyd, A. A.; Lesclaux, R. Peroxy radical kinetics resulting from the OH-initiated oxidation of 1,3-butadiene, 2,3-dimethyl-1,3-butadiene and isoprene. *J. Atmos. Chem.* **1998**, *29*, 267−298.
(30) Jenkin, M. E.; Hayman, G. D. Kinetics of reactions of primary, secondary and tertiary β-hydroxy peroxyl radicals: application to isoprene degradation. *J. Chem. Soc., Faraday Trans.* **1995**, *91*, 433−446.
(31) Dovrou, E.; Rivera-Rios, J. C.; Bates, K. H.; Keutsch, F. N. Sulfate formation via cloud processing from isoprene hydroxyl hydroperoxides (ISOPOOH). *Environ. Sci. Technol.* **2019**, *53*, 12476−12484.
(32) Dovrou, E.; Bates, K. H.; Rivera-Rios, J. C.; Cox, J. L.; Shutter, J. D.; Keutsch, F. N. Towards a chemical mechanism of the oxidation of aqueous sulfur dioxide via isoprene hydroxyl hydroperoxides (ISOPOOH). *Atmos. Chem. Phys.* **2021**, *21*, 8999−9008.
(33) Vasquez, K. T.; Crounse, J. D.; Schulze, B. C.; Bates, K. H.; Teng, A. P.; Xu, L.; Allen, H. M.; Wennberg, P. O. Rapid hydrolysis of tertiary isoprene nitrate efficiently removes NO_x from the atmosphere. *Proc. Natl Acad. Sci.* **2020**, *117*, 33011−33016.
(34) Taraborrelli, D.; Cabrera-Perez, D.; Bacer, S.; Gromov, S.; Lelieveld, J.; Sander, R.; Pozzer, A. Influence of aromatics on tropospheric gas-phase composition. *Atmos. Chem. Phys.* **2021**, *21*, 2615−2636.
(35) Müller, J.-F.; Stavrakou, T.; Peeters, J. Chemistry and deposition in the Model of Atmospheric composition at Global and Regional scales using Inversion Techniques for Trace gas Emissions (MAGRITTE v1.1) − Part 1: Chemical mechanism. *Geosci. Model Dev.* **2019**, *12*, 2307−2356.
(36) Taylor, W. D.; Allston, T. D.; Moscato, M. J.; Fazekas, G. B.; Kozlowski, R.; Takacs, G. A. Atmospheric photodissociation lifetimes for nitromethane, methyl nitrite, and methyl nitrate. *Int. J. Chem. Kinet.* **1980**, *12*, 231.
(37) Schwantes, R. H.; Charan, S. M.; Bates, K. H.; Huang, Y.; Nguyen, T. B.; Mai, H.; Kong, W.; Flagan, R. C.; Seinfeld, J. H. Low-volatility compounds contribute significantly to isoprene secondary organic aerosol (SOA) under high-NO_x conditions. *Atmos. Chem. Phys.* **2019**, *19*, 7255−7278.
(38) Kostenidou, E.; Pathak, R. K.; Pandis, S. N. An algorithm for the calculation of secondary organic aerosol density combining AMS and SMPS data. *Aerosol Sci. Technol.* **2007**, *41*, 1002−1010.
(39) Crounse, J. D.; McKinney, K. A.; Kwan, A. J.; Wennberg, P. O. Measurement of Gas-Phase Hydroperoxides by Chemical Ionization Mass Spectrometry. *Anal. Chem.* **2006**, *78*, 6726−6732.
(40) St. Clair, J. M.; McCabe, D. C.; Crounse, J. D.; Steiner, U.; Wennberg, P. O. Chemical Ionization Tandem Mass Spectrometer for the *In Situ* Measurement of Methyl Hydrogen Peroxide. *Rev. Sci. Instrum.* **2010**, *81*, 094102.
(41) Bates, K. H.; Crounse, J. D.; St. Clair, J. M.; Bennett, N. B.; Nguyen, T. B.; Seinfeld, J. H.; Stoltz, B. M.; Wennberg, P. O. Gas phase production and loss of isoprene epoxydiols. *J. Phys. Chem. A* **2014**, *118*, 1237−1246.
(42) Nguyen, T. B.; Tyndall, G. S.; Crounse, J. D.; Teng, A. P.; Bates, K. H.; Schwantes, R. H.; Coggon, M. M.; Zhang, L.; Feiner, P.; Miller, D. O.; Skog, K. M.; Rivera-Rios, J. C.; Dorris, M.; Olson, K. F.; Koss, A.; Wild, R. J.; Brown, S. S.; Goldstein, A. H.; de Gouw, J. A.; Brune, W. H.; Keutsch, F. N.; Seinfeld, J. H.; Wennberg, P. O. Atmospheric fates of Criegee intermediates in the ozonolysis of isoprene. *Phys. Chem. Chem. Phys.* **2016**, *18*, 10241−10254.
(43) Bates, K. H.; Nguyen, T. B.; Teng, A. P.; Crounse, J. D.; Kjaergaard, H. G.; Stoltz, B. M.; Seinfeld, J. H.; Wennberg, P. O. Production and fate of C_4 dihydroxycarbonyl compounds from isoprene oxidation. *J. Phys. Chem. A* **2016**, *120*, 106−117.
(44) Praske, E.; Crounse, J. D.; Bates, K. H.; Kurtén, T.; Kjaergaard, H. G.; Wennberg, P. O. Atmospheric fate of methyl vinyl ketone: peroxy radical reactions with NO and HO_2. *J. Phys. Chem. A* **2015**, *119*, 4562−4572.
(45) Su, T.; Chesnavich, W. J. Parametrization of the ion-polar molecule collision rate constant by trajectory calculations. *J. Chem. Phys.* **1982**, *76*, 5183−5185.
(46) Garden, A. L.; Paulot, F.; Crounse, J. D.; Maxwell-Cameron, I. J.; Wennberg, P. O.; Kjaergaard, H. G. Calculation of Conformationally Weighted Dipole Moments Useful in Ion-Molecule Collision Rate Estimates. *Chem. Phys. Lett.* **2009**, *474*, 45−50.
(47) Burkholder, J. B.; Sander, S. P.; Abbatt, J.; Barker, J. R.; Cappa, C.; Crounse, J. D.; Dibble, T. S.; Huie, R. E.; Kolb, C. E.; Kurylo, M. J.; Orkin, V. L.; Percival, C. J.; Wilmouth, D. M.; Wine, P. H. *Chemical Kinetics and Photochemical Data for Use in Atmospheric Studies, Evaluation No. 19*; JPL Publication 19−5, Jet Propulsion Laboratory, Pasadena, 2019 http://jpldataeval.jpl.nasa.gov.
(48) Atkinson, R.; Baulch, D. L.; Cox, R. A.; Crowley, J. N.; Hampson, R. F.; Hynes, R. G.; Jenkin, M. E.; Rossi, M. J.; Troe, J. IUPAC Task Group on Atmospheric Chemical Kinetic Data Evaluation. *Atmos. Chem. Phys.* **2004**, *4*, 1461−1738.
(49) Allen, H. M.; Teng, A. P.; Bates, K. H.; Crounse, J. D.; Thayer, M.; Rivera-Rios, J.; Keutsch, F.; St. Clair, J. M.; Wennberg, P. O. Kinetics and product yields of the OH driven oxidation of hydroxymethyl hydroperoxide. *J. Phys. Chem. A* **2018**, *122*, 6292−6302.
(50) York, D.; Evensen, N. M.; Martínez, M. L.; De Basabe Delgado, J. Unified Equations for the Slope, Intercept, and Standard Errors of the Best Straight Line. *Am. J. Phys.* **2004**, *72*, 367−375.
(51) Keller, C. A.; Long, M. S.; Yantosca, R. M.; Da Silva, A. M.; Pawson, S.; Jacob, D. J. HEMCO v1.0: a versatile, ESMF-compliant component for calculating emissions in atmospheric models. *Geosci. Model Dev.* **2014**, *7*, 1409−1417.
(52) Atkinson, R.; Baulch, D. L.; Cox, R. A.; Crowley, J. N.; Hampson, R. F.; Hynes, R. G.; Jenkin, M. E.; Rossi, M. J.; Troe, J.; IUPAC Subcommittee. Evaluated kinetic and photochemical data for atmospheric chemistry: Volume II − gas phase reactions of organic species. *Atmos. Chem. Phys.* **2006**, *6*, 3625−4055.
(53) St. Clair, J. M.; Rivera-Rios, J. C.; Crounse, J. D.; Knap, H. C.; Bates, K. H.; Teng, A. P.; Jörgensen, S.; Kjaergaard, H. G.; Keutsch, F. N.; Wennberg, P. O. Kinetics and Products of the Reaction of the First-Generation Isoprene Hydroxy Hydroperoxide (ISOPOOH) with OH. *J. Phys. Chem. A* **2016**, *120*, 1441−1451.
(54) Möller, K. H.; Bates, K. H.; Kjaergaard, H. G. The importance of peroxy radical hydrogen-shift reactions in atmospheric isoprene oxidation. *J. Phys. Chem. A.* **2019**, *123*, 920−932.
(55) Jenkin, M. E.; Valorso, R.; Aumont, B.; Rickard, A. R. Estimation of rate coefficients and branching ratios for reactions of organic peroxy radicals for use in automated mechanism construction. *Atmos. Chem. Phys.* **2019**, *19*, 7691−7717.
(56) Cavalli, F.; Barnes, I.; Becker, K.-H. FT-IR kinetic and product study of the OH radical and Cl-atom−initiated oxidation of dibasic esters. *Int. J. Chem. Kinet.* **2001**, *33*, 431−439.
(57) Crounse, J. D.; Knap, H. C.; Örnsö, K. B.; Jörgensen, S.; Paulot, F.; Kjaergaard, H. G.; Wennberg, P. O. Atmospheric fate of methacrolein. 1. Peroxy radical isomerization following addition of OH and O_2. *J. Phys. Chem. A* **2012**, *116*, 5756−5762.
(58) Lee, L.; Teng, A. P.; Wennberg, P. O.; Crounse, J. D.; Cohen, R. C. On rates and mechanisms of OH and O_3 reactions with isoprene-derived hydroxy nitrates. *J. Phys. Chem. A* **2014**, *118*, 1622−1637.
(59) Lightfoot, P. D.; Cox, R. A.; Crowley, J. N.; Destriau, M.; Hayman, G. D.; Jenkin, M. E.; Moortgat, G. K.; Zabel, F. Organic peroxy radicals: kinetics, spectroscopy and tropospheric chemistry. *Atmos. Environ.* **1992**, *26A*, 1805−1964.
(60) Matsunaga, A.; Ziemann, P. J. Yields of β-hydroxynitrates and dihydroxynitrates in aerosol formed from OH radical initiated reactions of linear alkenes in the presence of NO_x. *J. Phys. Chem. A* **2009**, *113*, 599−606.
(61) Matsunaga, A.; Ziemann, P. J. Yields of beta-hydroxynitrates, dihydroxynitrates, and trihydroxynitrates formed from OH radical-initiated reactions of 2-methyl-1-alkenes. *Proc. Natl. Acad. Sci.* **2010**, *107*, 6664−6669.

(62) Picquet-Varrault, B.; Doussin, J.-F.; Durand-Jolibois, R.; Carlier, P. FTIR spectroscopic study of the OH-induced oxidation of two linear acetates: ethyl and n-propyl acetates. *Phys. Chem. Chem. Phys.* **2001**, *3*, 2595−2606.
(63) Picquet-Varrault, B.; Doussin, J.-F.; Durand-Jolibois, R.; Carlier, P. FTIR spectroscopic study of the OH-induced oxidation of isopropyl, isobutyl, and *tert*-butyl acetates. *J. Phys. Chem. A* **2002**, *106*, 2895−2902.
(64) Pimentel, A. S.; Tyndall, G. S.; Orlando, J. J.; Hurley, M. D.; Wallington, T. J.; Sulbaek Andersen, M. P.; Marshall, P.; Dibble, T. S. Atmospheric chemistry of isopropyl formate and *tert*-butyl formate. *Int. J. Chem. Kinet.* **2010**, *42*, 479−498.
(65) Teng, A. P.; Crounse, J. D.; Lee, L.; St. Clair, J. M.; Cohen, R. C.; Wennberg, P. O. Hydroxy nitrate production in the OH-initiated oxidation of alkenes. *Atmos. Chem. Phys.* **2015**, *15*, 4297−4316.
(66) Tuazon, E. C.; Aschmann, S. M.; Atkinson, R.; Carter, W. P. L. The Reactions of Selected Acetates with the OH Radical in the Presence of NO: Novel Rearrangement of Alkoxy Radicals of Structure RC(O)OCH(Ȯ)R̆. *J. Phys. Chem. A* **1998**, *102*, 2316−2321.
(67) Tuazon, E. C.; Aschmann, S. M.; Atkinson, R. Products of the gas-phase reactions of the OH radical with 1-methoxy-2-propanol and 2-butoxyethanol. *Environ. Sci. Technol.* **1998**, *32*, 3336−3345.
(68) Yeh, G. K.; Ziemann, P. J. Identification and yields of 1,4-hydroxynitrates formed from the reactions of C_8-C_{16} *n*-alkanes with OH radicals in the presence of NO_x. *J. Phys. Chem. A* **2014**, *118*, 8797−8157.
(69) Jenkin, M. E.; Hurley, M. D.; Wallington, T. J. Investigation of the Radical Product Channel of the $CH_3C(O)CH_2O_2$ + HO_2 Reaction in the Gas Phase. *Phys. Chem. Chem. Phys.* **2008**, *10*, 4274−4280.
(70) Jenkin, M. E.; Hurley, M. D.; Wallington, T. J. Investigation of the Radical Product Channel of the $CH_3OCH_2O_2$ + HO_2 Reaction in the Gas Phase. *J. Phys. Chem. A* **2010**, *114*, 408−416.
(71) Hasson, A. S.; Tyndall, G. S.; Orlando, J. J.; Singh, S.; Hernandez, S. Q.; Campbell, S.; Ibarra, Y. Branching Ratios for the Reaction of Selected Carbonyl-Containing Peroxy Radicals with Hydroperoxy Radicals. *J. Phys. Chem. A* **2012**, *116*, 6264−6281.
(72) Krechmer, J. E.; Coggon, M. M.; Massoli, P.; Nguyen, T. B.; Crounse, J. D.; Hu, W.; Day, D. A.; Tyndall, G. S.; Henze, D. K.; Rivera-Rios, J. C.; Nowak, J. B.; Kimmel, J. R.; Mauldin, R. L., III; Stark, H.; Jayne, J. T.; Sipilä, M.; Junninen, H.; St. Clair, J. M.; Zhang, X.; Feiner, P. A.; Zhang, L.; Miller, D. O.; Brune, W. H.; Keutsch, F. N.; Wennberg, P. O.; Seinfeld, J. H.; Worsnop, D. R.; Jimenez, J. L.; Canagaratna, M. R. Formation of Low Volatility Organic Compounds and Secondary Organic Aerosol from Isoprene Hydroxyhydroperoxide Low-NO Oxidation. *Environ. Sci. Technol.* **2015**, *49*, 10330−10339.
(73) Liu, J.; D'Ambro, E. L.; Lee, B. H.; Lopez-Hilfiker, F. D.; Zaveri, R. A.; Rivera-Rios, J. C.; Keutsch, F. N.; Iyer, S.; Kurten, T.; Zhang, Z.; Gold, A.; Surratt, J. D.; Shilling, J. E.; Thornton, J. A. Efficient Isoprene Secondary Organic Aerosol Formation from a Non-IEPOX Pathway. *Environ. Sci. Technol.* **2016**, *50*, 9872−9880.
(74) Compernolle, S.; Ceulemans, K.; Müller, J.-F. EVAPORATION: a new vapour pressure estimation methodfor organic molecules including non-additivity and intramolecular interactions. *Atmos. Chem. Phys.* **2011**, *11*, 9431−9450.
(75) Crounse, J. D.; Paulot, F.; Kjaergaard, H. G.; Wennberg, P. O. Peroxy radical isomerization in the oxidation of isoprene. *Phys. Chem. Chem. Phys.* **2011**, *13*, 13607−13613.
(76) Nguyen, T. B.; Crounse, J. D.; Schwantes, R. H.; Teng, A. P.; Bates, K. H.; Zhang, X.; St. Clair, J. M.; Brune, W. H.; Tyndall, G. S.; Keutsch, F. N.; Seinfeld, J. H.; Wennberg, P. O. Overview of the Focused Isoprene eXperiment at the California Institute of Technology (FIXCIT): mechanistic chamber studies on the oxidation of biogenic compounds. *Atmos. Chem. Phys.* **2014**, *14*, 13531−13549.
(77) Zhang, X.; Cappa, C. D.; Jathar, S. H.; McVay, R. C.; Ensberg, J. J.; Kleeman, M. J.; Seinfeld, J. H. Influence of vapor wall loss in laboratory chambers on yields of secondary organic aerosol. *Proc. Natl. Acad. Sci.* **2014**, *111*, 5802−5807.
(78) Zhang, X.; Schwantes, R. H.; McVay, R. C.; Lignell, H.; Coggon, M. M.; Flagan, R. C.; Seinfeld, J. H. Vapor wall deposition in Teflon chambers. *Atmos. Chem. Phys.* **2015**, *15*, 4197−4214.
(79) Neeb, P.; Sauer, F.; Horie, O.; Moortgat, G. K. Formation of hydroxymethyl hydroperoxide and formic acid in alkene ozonolysis in the presence of water vapour. *Atmos. Environ.* **1997**, *31*, 1417−1423.
(80) Liggio, J.; Li, S.-M.; McLaren, R. Reactive uptake of glyoxal by particulate matter. *J. Geophys. Res.* **2005**, *110*, D10304.
(81) Galloway, M. M.; Chhabra, P. S.; Chan, A. W. H.; Surratt, J. D.; Flagan, R. C.; Seinfeld, J. H.; Keutsch, F. N. Glyoxal uptake on ammonium sulphate seed aerosol: reaction products and reversibility of uptake under dark and irradiated conditions. *Atmos. Chem. Phys.* **2009**, *9*, 3331−3345.
(82) Cope, J. D.; Abellar, K. A.; Bates, K. H.; Fu, X.; Nguyen, T. B. Aqueous Photochemistry of 2-Methyltetrol and Erythritol as Sources of Formic Acid and Acetic Acid in the Atmosphere. *ACS Earth Space Chem.* **2021**, *5*, 1265−1277.
(83) Nguyen, T. B.; Crounse, J. D.; Teng, A. P.; St. Clair, J. M.; Paulot, F.; Wolfe, G. M.; Wennberg, P. O. Rapid deposition of oxidized biogenic compounds to a temperate forest. *Proc. Natl. Acad. Sci.* **2015**, *112*, E392−E401.
(84) Stavrakou, T.; Müller, J.-F.; Peeters, J.; Razavi, A.; Clarisse, L.; Clerbaux, C.; Coheur, P.-F.; Hurtmans, D.; De Mazière, M.; Vigouroux, C.; Deutscher, N. M.; Griffith, D. W. T.; Jones, N.; Paton-Walsh, C. Satellite Evidence for a Large Source of Formic Acid from Boreal and Tropical Forests. *Nat. Geosci.* **2012**, *5*, 26−30.
(85) Millet, D. B.; Baasandorj, M.; Farmer, D. K.; Thornton, J. A.; Baumann, K.; Brophy, P.; Chaliyakunnel, S.; de Gouw, J. A.; Graus, M.; Hu, L.; Koss, A.; Lee, B. H.; Lopez-Hilfiker, F. D.; Neuman, J. A.; Paulot, F.; Peischl, J.; Pollack, I. B.; Ryerson, T. B.; Warneke, C.; Williams, B. J.; Xu, J. A Large and Ubiquitous Source of Atmospheric Formic Acid. *Atmos. Chem. Phys.* **2015**, *15*, 6283−6304.
(86) Link, M. F.; Nguyen, T. B.; Bates, K.; Müller, J.-F.; Farmer, D. K. Can Isoprene Oxidation Explain High Concentrations of Atmospheric Formic and Acetic Acid over Forests? *ACS Earth Space Chem.* **2020**, *4*, 730−740.

https://doi.org/10.1021/acs.est.1c04177
Environ. Sci. Technol. 2021, 55, 14294−14304